Microchimica Acta (2023) 190:243
https://doi.org/10.1007/s00604-023-05822-y

ORIGINAL PAPER

Mn_3O_4 nanoparticles decorated porous reduced graphene oxide with excellent oxidase-like activity for fast colorimetric detection of ascorbic acid

Dong Peng[1] · Mingming Que[1] · Xiulong Deng[1] · Qifang He[1] · Yuhong Zhao[1] · Shuzhen Liao[1] · Xun Li[1] · Hongdeng Qiu[1,2]

Received: 23 November 2022 / Accepted: 4 May 2023 / Published online: 29 May 2023

Abstract

Mn_3O_4 nanoparticles composed of porous reduced graphene oxide nanosheets (Mn_3O_4@p-rGO) with enhanced oxidase-like activity were successfully fabricated through an in-situ approach for fast colorimetric detection of ascorbic acid (AA). The residual Mn^{2+} in the GO suspension of Hummers method was directly reused as the manganese source, improving the atom utilization efficiency. Benefiting from the uniform distribution of Mn_3O_4 nanoparticles on the surface of p-rGO nanosheets, the nanocomposite exhibited larger surface area, more active sites, and accelerated electron transfer efficiency, which enhanced the oxidase-like activity. Mn_3O_4@p-rGO nanocomposite efficiently activate dissolved O_2 to generate singlet oxygen ($^1O_2$), leading to high oxidation capacity toward the substrate 3,3′,5,5′–tetramethylbenzidine (TMB) without the extra addition of H_2O_2. Furthermore, the prominent absorption peak of the blue ox-TMB at 652 nm gradually decreased in the presence of AA, and a facile and fast colorimetric sensor was constructed with a good linear relationship (0.5–80 μM) and low LOD (0.278 μM) toward AA. Owing to the simplicity and excellent stability of the sensing platform, its practical application for AA detection in juices has shown good feasibility and reliability compared with HPLC and the 2, 4-dinitrophenylhydrazine colorimetric method. The oxidase-like Mn_3O_4@p-rGO provides a versatile platform for applications in food testing and disease diagnosis.

Keywords Mn_3O_4 nanoparticles · Porous reduced graphene oxide · Oxidase-like activity · Nanozyme · Ascorbic acid detection · Colorimetry

Introduction

Ascorbic acid (AA) is an important biological cofactor and antioxidant, which participate in various biochemical and physiological processes [1]. Abnormal levels of AA are associated with scurvy, cancer, cardiovascular disease, and some mental illness [2–5]. It is of great importance to develop convenient and rapid methods for AA detection with high sensitivity in a vast range of areas such as drugs, foods, and clinical diagnosis. Recently, various methods have been exploited for AA determination, including high-performance liquid chromatography (HPLC), capillary electrophoresis, electrochemistry, chemiluminescence, and fluorescence [6–12]. Colorimetric assay has emerged as an important sensing platform due to its rapidity, simplicity, low-cost and easy detection by naked eyes. Nowadays, enzyme-like nanomaterials-based sensors have drawn great interest as colorimetric tools [13].

Nanozyme is a class of nanomaterials that possess intrinsic enzyme-like properties, which can be applied as an enzyme substitute to catalyze the biochemical reactions of the substrates under physiological conditions [14]. Owning to the advantages of low cost, high stability, and ease of production, nanozyme has excellent prospects in molecular detection and some other areas. The peroxidase

Dong Peng and Mingming Que contributed equally to this work.

✉ Hongdeng Qiu
hdqiu@licp.cas.cn

[1] School of Chemistry and Chemical Engineering, Gannan Normal University, Ganzhou 341000, China

[2] CAS Key Laboratory of Chemistry of Northwestern Plant Resources and Key Laboratory for Natural Medicine of Gansu Province, Lanzhou Institute of Chemical Physics, Chinese Academy of Sciences, Lanzhou 730000, China

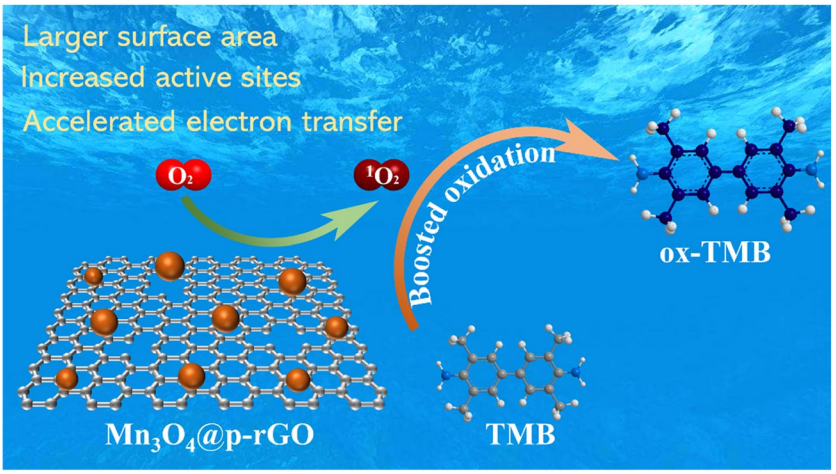

Scheme 1 Schematic illustration the mechanism the boosted oxidase-like activity of Mn_3O_4@p-rGO

and oxidase-like nanomaterials can efficiently catalyze the oxidation of colorless substrates to produce colored products, which can be used as colorimetric sensors [15, 16]. Different from peroxidase-mimics, oxidase-mimicking nanozymes can directly use dissolved oxygen molecules as the oxidant [17]. Herein, the oxidase-mimics are much more attractive in biosensing, which can effectively eliminate the interferences of the extra addition of H_2O_2. Most of the reported oxidase-mimics concerned in metal oxide nanoparticles and noble metal nanoparticles [15], such as Au [18], Pt[19], CeO_2 [20], NiO [21], MnO_2 [22], Mn_3O_4 [23], and V_2O_5 nanozymes [24]. However, the catalytic activities of these metal nanomaterials are severely deteriorated by the spontaneous aggregation and instability. Improving the catalytic activity and stability of the nanoparticle-based nanozyme is still challenging.

The growth of nanoparticles on specific support can efficiently prevent aggregation and increase active sites, which is an effective strategy to enhance the catalytic activity [25–27]. Graphene nanosheets, as an excellent two-dimensional (2D) carbon support, is regarded as a promising candidate due to the characteristics of high mechanical strength, large surface area, high chemical stability, and good biocompatibility [28–30]. However, the agglomeration and restacking of graphene sheets can lead the decrease of active sites. Porous graphene, which possesses abundant pores on the surface, could efficiently avoid agglomeration and increase the surface area [31–34]. We have proposed several strategies to deposit different nanoparticles (including TiO_2 nanoparticles, Fe/Ni bimetallic nanoparticles, Zn-BTC MOF, and so on) on the surface of porous graphene, which exhibited good potential applications in organic pollutant degradation [35], rare earth adsorption [36, 37], separation [38], and molecule detection [39].

In this work, we successfully combined porous reduced graphene oxide nanosheets (p-rGO) with Mn_3O_4 nanoparticles (Mn_3O_4@p-rGO) through an in-situ fabrication strategy. Mn_3O_4 nanoparticles were synthesized by reusing the absorbed Mn^{2+} on the surface of GO as the precursor, and the p-rGO with porous structure was obtained by directly calcinating in open air. The decoration of Mn_3O_4 nanoparticles on the surface of p-rGO nanosheets effectively enhanced the oxidase-like activity owing to the larger surface area, more active sites, and accelerated electron transfer efficiency (as shown in Scheme 1). Furthermore, a simple and fast colorimetric sensor was constructed for AA detection with satisfactory sensitivity and selectivity. It's proved that Mn_3O_4@p-rGO is a promising oxidase alternative with potential applications in molecular sensing and disease diagnosis.

Experimental section

Preparation of Mn_3O_4@p-rGO nanocomposites

Aqueous graphite oxide dispersion was prepared via the modified Hummers method [40]. Specifically, with stirring in an ice bath, graphite flakes (0.5 g), and $NaNO_3$ (0.5 g) was added to 25 mL concentrated H_2SO_4. $KMnO_4$ (3 g) was then slowly added with the temperature of the suspension lower than 20 °C throughout the process. After 2 h, the mixture was transferred to a 40 °C water bath for an additional hour. Subsequently, 40 mL of H_2O was added dropwise to increase the temperature. The reaction was performed at 90 °C for 0.5 h and followed by further addition of 5 mL H_2O_2. Then, the mixture was centrifuged to remove the soluble ions, and 5 M KOH solution was added to neutralize the products. Let stand for 1 h, the black precipitates were washed with water for three

times and dried in vacuum at 60 °C. At last, the samples were rapidly transferred to a muffle furnace at 500 °C for 10 min, and the final product was collected and denoted as Mn_3O_4@p-rGO nanocomposite.

Oxidase-mimic activity assay

The oxidase-mimic activity was evaluated by using TMB as a chromogenic substrate. Typically, 20 μL of TMB (10 mM), 30 μL of Mn_3O_4@p-rGO nanocomposites (100 mg/L), and 40 μL of acetate buffer (100 mM, pH 4.0) were mixed with 110 mL DI water, and the absorbance spectrum was recorded after incubated for 10 min. The kinetic assays were performed by changing the TMB concentrations (0.025, 0.05, 0.075, 0.1, 0.15, 0.2, 0.3, 0.4, 0.5, 0.6, and 0.7 mM) in the reaction mixtures. All reaction solutions were incubated at room temperature (25 ℃) unless otherwise stated, and the absorbance at 652 nm was recorded at 1-s interval over 5 min. All data were collected with three independent measurements.

Detection of AA

For colorimetric detection of AA, 30 μL of Mn_3O_4@p-rGO nanocomposites solution (100 mg/L), 40 μL of acetate buffer (100 mM, pH 4.0), and various concentrations of AA (final concentrations: 0–100 μM) were mixed in a 0.5-mL tube. Then, 20 μL of TMB (10 mM) solution was added, and further diluted with ultrapure water to a final volume of 200 μL. These mixtures were incubated for 10 min, and then the UV–vis absorbance spectrum was recorded. Similarly, the interference experiment was performed by replacing AA with some other agents. All data were collected with three independent measurements.

Detection AA in fruit juice

Fresh fruits were purchased from market, and the edible part of these fruits were isolated. Then, the fruit juices were obtained with an electric juicer, the juice were centrifuged at 3000 rpm for 10 min to remove the fruit residues. The supernatants were collected and diluted tenfold with 100 mM acetate buffer (pH 4.0) and stored at 4 ℃. Under the detection procedures, 20 μL of the diluted juices were added into the reaction systems, and further detected as mentioned above. Totally, all fruit juices were diluted 100-fold to fit the sensing response range. The AA concentrations in these samples were also detected by HPLC method and 2, 4-dinitrophenylhydrazine colorimetry method according to the Chinese standard GB 5009.86–2016. All data were collected with three independent measurements.

Results and discussion

Characterizations of Mn_3O_4@p-rGO nanocomposites

As illustrated in Fig. 1A, a facile in-situ fabrication strategy was applied for the synthesis of the Mn_3O_4@p-rGO nanocomposites. Firstly, Mn^{2+}-GO suspension was obtained by the modified Hummers method. Under this process, $KMnO_4$ was both used as a strong oxidant for graphite oxidation and as the manganese source. Mn^{2+} ions were absorbed on the surface of GO nanosheets, on account of the strong coordination interaction of the oxygen containing groups on the GO nanosheets. After being neutralized with KOH and exposed in air, the absorbed Mn^{2+} was in situ converted into Mn_3O_4 nanoparticles [41]. After calcination under high temperature in open air for a short time, the GO nanosheets were oxidized to form porous structure as confirmed by the characterizations of the morphology and structure of the nanocomposites as follows.

As displayed in Fig. 1B, the porous structure of p-rGO nanosheets can be easily identified from the TEM image, and the Mn_3O_4 nanoparticles uniformly distributed on the surface of p-rGO nanosheets. The p-rGO provided a great support for the formation of the small Mn_3O_4 nanoparticles and prevent them from aggregation. On the other hand, Mn_3O_4 nanoparticles also protect the p-rGO nanosheets from burning up at high temperature in open air. The typical (101) crystal plane of Mn_3O_4 nanoparticles can be observed from the crystal plane spacing of 0.49 nm [26]. As shown in Fig. 1C, the typical diffraction peaks in the XRD pattern of the nanocomposites match well with the standard hausmannite structure of Mn_3O_4 (JCPDS no. 24–0734), suggesting the high purity of the Mn_3O_4 nanoparticles [26, 42]. Besides, the broad peak at around 24° implied the existence of the (002) plane of the porous graphene nanosheets. In the Raman spectra of the nanocomposites (Fig. S1), the intensity ratio between the D and G bonds (I_D/I_G) was 1.05, implying the enhanced electron conductivity [43]. Moreover, the prominent peak at 647 cm^{-1} associated with the phonon lines of Mn_3O_4 [42, 43]. Thus, the successful composition of p-rGO nanosheets and Mn_3O_4 nanoparticles is confirmed.

Furthermore, XPS was performed to study the electronic structure and surface composition of the Mn_3O_4@p-rGO nanocomposites. The XPS survey spectrum (Fig. 1D) reveals the presence of Mn, C, and O elements in the nanocomposites. As shown in the high-resolution Mn 2p spectrum (Fig. S2A), there are two distinct peaks at 641.8 (Mn $2p_{3/2}$) and 653.6 eV (Mn $2p_{1/2}$) with a spin-energy separation of 11.8 eV, which agrees well with the earlier reported Mn_3O_4 [26, 44]. The C 1 s spectrum (Fig. S2B)

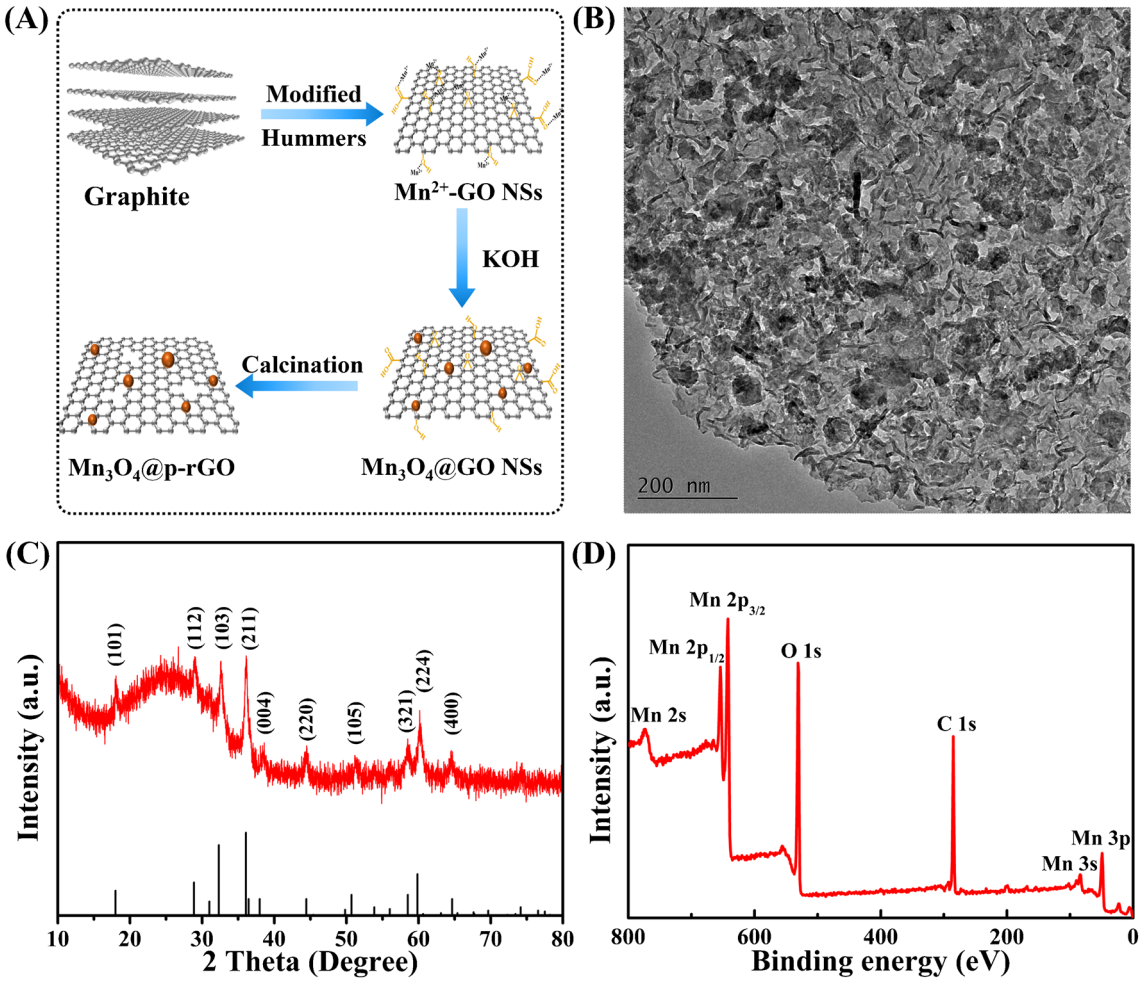

Fig. 1 **A** Schematic illustration of fabrication process of Mn_3O_4@p-rGO. **B** TEM image of Mn_3O_4@p-rGO nanocomposites. **C** XRD pattern and **D** XPS spectrum of Mn_3O_4@p-rGO nanocomposites

can be deconvoluted into four components at 284.8, 286.6, 288.2, and 289.1 eV, which correspond to the C–C/C = C, C-O, C = O, and O-C = O bonds, respectively [42]. Most of the oxygen atoms in the surface of porous graphene may residue from GO. As shown in Fig. S2C, the O 1 s spectrum reveals the presence of Mn–O-Mn (530.2 eV), Mn-OH (531.5 eV), and C-O/C = O (532.8 eV), which are consistent well with the previous results [42]. Overall, the Mn_3O_4 nanoparticles were successfully deposited on the surface of p-rGO.

Enzyme mimicking activity

The typical chromogenic substrates (TMB, ABTS, and OPD) were selected to test the oxidase-like performance of Mn_3O_4@p-rGO nanocomposites. As displayed in Fig. 2A and Fig. S3, all of these substrates were oxidized to generate the chromatic products with the characteristic UV–vis absorption spectra under the presence of Mn_3O_4@p-rGO. Besides, the obvious color change can be observed, suggesting the versatile applicability of Mn_3O_4@p-rGO as an oxidase mimic. To further evaluate the oxidase-mimic activity, TMB was selected as the model substrate, and the absorbance intensity at 652 nm ($A_{652\ nm}$) was monitored to assess the catalytic performance. As shown in Fig. 2B, the catalytic kinetics of different catalysts were investigated. Notably, the oxidase activity of the catalysts follows the order: Mn_3O_4@p-rGO > Mn_3O_4@GO > Mn_3O_4 > p-rGO. Interestingly, the catalytic activity of Mn_3O_4@p-rGO nanocomposites is higher than the sum of the individual catalytic activity of Mn_3O_4 and p-rGO, exhibiting a good synergistic effect. Thus, the Mn_3O_4 nanoparticles decorated on p-rGO exhibited the highest oxidase activity, which was selected as the best oxidase-mimic excellent candidate. As previously reported, both GO and p-rGO were applied as the supports for boosting the catalytic activities of nanoparticles, owing to the increased surface area and catalytic sites [30, 45, 46]. Herein, the

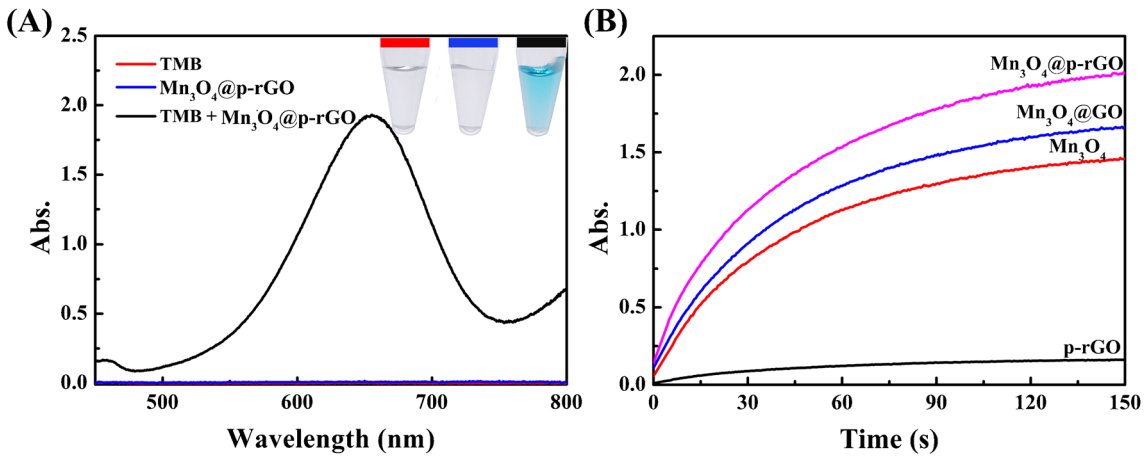

Fig. 2 **A** UV−vis absorption spectra of different reaction systems (inset: photographs of different reaction systems); **B** time-dependent absorbance changes under the presence of different catalysts. All data were represented as means ± standard deviation of three independent measurements

catalytic activity of Mn_3O_4@p-rGO was superior to that of Mn_3O_4@GO, which may mainly attribute to the better electron transfer ability of p-rGO.

Furthermore, the effects of catalyst concentration, reaction pH, temperature, and storage time on the catalytic activity of the nanozyme were evaluated. As shown in Fig. S4A and S4B, 15 mg/L of Mn_3O_4@p-rGO and pH = 4.0 were optimized as the best reaction conditions. The catalytic activity of Mn_3O_4@p-rGO peaked at 45 ℃ over the range of 15–65 ℃ (Fig. S4C). To facilitate the practical application, the following experiments were carried out at 25 ℃. Besides, the catalytic activity of the nanozyme exhibited no apparent change even after store for four months (Fig. S4D), suggesting its outstanding stability.

To evaluate the oxidase-mimic activity of Mn_3O_4@p-rGO, the steady-state kinetic parameters were further analyzed. By monitoring the catalytic reaction velocity (V) with the addition of different concentrations of TMB, the obtained plot follows the typical Michaelis–Menten curve (Fig. 3A). The Michaelis constant (K_m) and maximum initial velocity (V_{max}) were calculated to be 0.1135 mM and 164.5×10^{-8} M s^{-1}, respectively. Compared with most reported oxidase-mimics (including Mn_3O_4 nanomaterials with different morphologies and some other nanoparticle-decorated graphene nanocomposites), Mn_3O_4@p-rGO had a comparable K_m value and higher V_{max} (Table S1), suggesting that Mn_3O_4@p-rGO has a high affinity toward TMB and excellent oxidase-mimic activity.

Oxidase-mimic nanozymes can catalyze the substrates oxidation in the presence of dissolved O_2 as the electron acceptor. Hence, the catalytic activity of Mn_3O_4@p-rGO in N_2/O_2-saturated solution was studied. As shown in Fig. 3B, the catalytic activity increased obviously after the solution was purged with O_2, while it was inhibited under a N_2-saturated solution. Thus, the dissolved O_2 participated in the oxidation of TMB.

To further figure out the possible mechanism, different kinds of radical scavengers were used to verify the possible reactive oxygen species (ROS, including hydroxyl radical (·OH), singlet oxygen atom ($^1O_2$), and superoxide radical (O_2^-)) involving the catalytic process. As shown in Fig. 3C, TBA (·OH scavenger) and *p*-benzoquinone (O_2^- scavenger) exhibited weak effects on the catalytic activity even at high concentrations, suggesting that there was almost no ·OH and O_2^- generated in the reaction system. Obviously, the catalytic activity was sharply reduced with the addition of NaN_3 ($^1O_2$ scavenger), indicating the generation of plenty of $^1O_2$ in the solution. Furthermore, the existence of these reactive oxygen species was investigated by ESR technology, DMPO and TEMP were used as the spin-trapping reagents for the capture of O_2^- or ·OH, and $^1O_2$, respectively. As shown in Fig. S5, the weak EPR signals attributed to O_2^- and ·OH confirmed the absence of O_2^- or ·OH in the reaction solution. In contrast, the strong triplet EPR peaks of TEMPOL verified the existence abundant of $^1O_2$ free radicals (Fig. 3D).

Based on these results, the possible catalytic mechanism for TMB oxidation can be illustrated as follows: the dissolved O_2 efficiently adsorbed on the mesoporous structure of p-rGO, and then it was immediately activated to generate $^1O_2$ by the increasing active sites of Mn_3O_4 nanoparticles. Subsequently, the generated $^1O_2$ with strong oxidizing ability immediately oxidized TMB to the blue ox-TMB.

Colorimetric detection of AA

AA is a kind of typical antioxidant, which widely exist in fruit. With the addition of AA in the Mn_3O_4@p-rGO-TMB

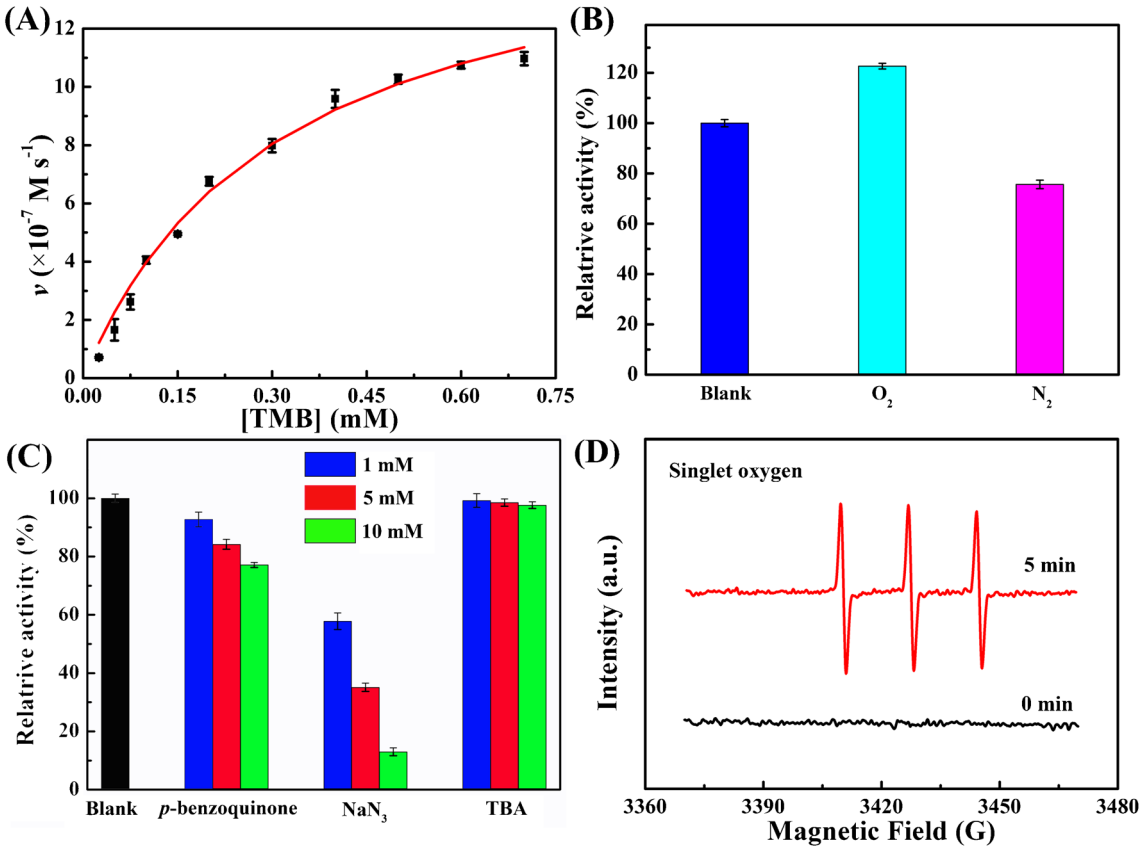

Fig. 3 **A** Steady-state kinetic assay of Mn_3O_4@p-rGO on TMB oxidation. **B** Catalytic performance of Mn_3O_4@p-rGO in N_2/O_2-saturated conditions. **C** The effects of different radical scavengers on the catalytic activity of Mn_3O_4@p-rGO. **D** EPR spectra for detection of $^1O_2$ before and after reaction for 5 min. All data were represented as means ± standard deviation of three independent measurements

reaction system, the generated $^1O_2$ can be directly eliminated by AA, which greatly inhibits the chromogenic reaction of TMB. Meanwhile, the blue ox-TMB can also be transformed into colorless TMB in the existence of AA. Based on this principle and the excellent oxidase enzyme mimic activity of Mn_3O_4@p-rGO nanocomposites, a fast, sensitive assay could be established. As displayed in Fig. 4 A, with the increase of AA concentration (0–100 μM), the absorbance of ox-TMB gradually decreased, and the color of the solution fading dark blue to colorless. The absorption differences at 652 nm (ΔA_{652}) were further calculated, which exhibited good linearity to the AA concentrations in the range of 0.5 μM to 80 μM (inset of Fig. 4B). The limit of detection (LOD) for AA was calculated to be 0.278 μM according to the 3σ/m criterion (where σ is the standard deviation of the blank and m is the slope of the calibration plot). The proposed Mn_3O_4@p-rGO-TMB sensing platform exhibited higher sensitivity and wider sensing range than most of the reported probes (Table S2). Additionally, compared with the peroxidase-mimic probes, the proposed sensing platform is much easier to operate and facilitates the application in complex conditions.

To further assess the selectivity of the Mn_3O_4@p-rGO-TMB detection system toward AA, the potential effects of different interferential substances (such as citric acid, benzoic acid, adipic acid, uric acid, and some amino acids) were measured. As shown in Fig. 4C, the presence of these interferential substances has no influence on the detection of AA, and no obvious color change can be observed even in a much higher concentration.

The practical usability of Mn_3O_4@p-rGO for AA detection was carried out in some different fresh fruits, such as pitaya, grape, and navel orange. As displayed in Table S3, the contents of AA in these fruits juice were determined, and the standard addition method was applied by adding different amounts of AA in the solution. The recoveries of the samples range from 97.8 to 104.2%, indicating the feasibility and reliability of the proposed method for AA determination in practical samples. Furthermore, HPLC method and 2,4-dinitrophenylhydrazine colorimetry method were also applied to detect the concentrations of the fruit juices. As listed in Table S4, the detected concentrations by our method were consistent with

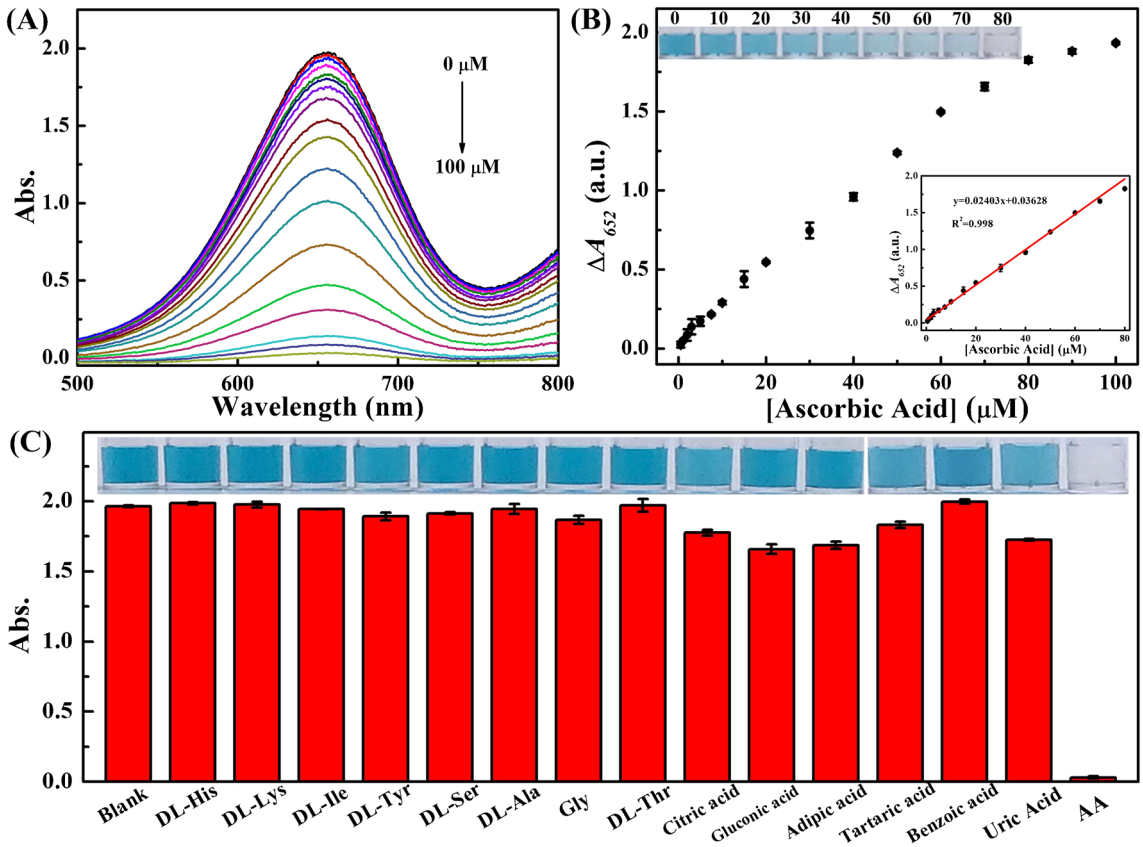

Fig. 4 **A** Adsorption spectra of the Mn_3O_4@p-rGO-TMB reaction system with different concentrations of AA (0, 0.5, 1, 2, 3, 5, 7.5, 10, 15, 20, 30,40, 50, 60, 70, 80, 90, and 100 μM). **B** Absorbance difference ($\Delta A_{652} = A - A_0$,) under the presence of different amount of AA; inset: the linear calibration plot of ΔA_{652} against the AA concentration (0.5–80 μM), and the visual picture corresponding to the AA concentrations. **C** Interference of different agents for detection of AA, the concentration of these interfere agents were 250 μM, and AA was 100 μM; inset: corresponding photographs of the reaction solutions. All data were represented as means ± standard deviation of three independent measurements

these reference methods, indicating the as-prepared method presented acceptable precision and accuracy.

Conclusions

The Mn_3O_4@p-rGO nanocomposite was successfully prepared through an in-situ fabrication strategy. Owning to the synergistic effect between Mn_3O_4 nanoparticles and p-rGO nanosheets, the hybrid exhibited enhanced oxidase-like activity compared with Mn_3O_4 nanoparticles or p-rGO nanosheets alone. A simple and fast colorimetric sensor of Mn_3O_4@p-rGO-TMB detection system was constructed for AA detection with excellent sensitivity and selectivity. Furthermore, practical application for AA detection in real samples also demonstrated its good feasibility and reliability. This work indicates the decoration of nanoparticles on specific support is an efficient strategy to enhance their enzyme-like activities, which exhibit promising potential in food safety, pharmacy, biosensing, and disease diagnosis.

Supplementary Information The online version contains supplementary material available at https://doi.org/10.1007/s00604-023-05822-y.

Funding The work was supported by the National Natural Science Foundation of China (21964003), the Science and Technology Project of the Education Department of Jiangxi Province (490042), the Double Thousand Talents Program of Jiangxi Province (jxsq2019102009), and the College Students' Innovation and Entrepreneurship Projects of Gannan Normal University (CX220058).

Declarations

Conflict of interest The authors declare no competing interests.

References

1. Chen Q, Espey MG, Sun AY, Pooput C, Kirk KL, Krishna MC, Khosh DB, Drisko J, Levine M (2008) Pharmacologic doses of ascorbate act as a prooxidant and decrease growth of aggressive tumor xenografts in mice. P Natl Acad Sci USA 105(32):11105–11109

2. Padayatty SJ, Riordan HD, Hewitt SM, Katz A, Hoffer LJ, Levine M (2006) Intravenously administered vitamin C as cancer therapy: three cases. Can Med Assoc J 174(7):937–942
3. Padayatty SJ, Katz A, Wang Y, Eck P, Kwon O, Lee J-H, Chen S, Corpe C, Dutta A, Dutta SK, Levine M (2003) Vitamin C as an Antioxidant: Evaluation of Its Role in Disease Prevention. J Am Coll Nutr 22(1):18–35
4. Sönmez M, Türk G, Yüce A (2005) The effect of ascorbic acid supplementation on sperm quality, lipid peroxidation and testosterone levels of male Wistar rats. Theriogenology 63(7):2063–2072
5. Massey LK, Liebman M, Kynast-Gales SA (2005) Ascorbate increases human oxaluria and kidney stone risk. J Nutr 135(7):1673–1677
6. Nováková L, Solich P, Solichová D (2008) HPLC methods for simultaneous determination of ascorbic and dehydroascorbic acids. Trac-trend Anal Chem 27(10):942–958
7. Ma Y, Zhou M, Jin X, Zhang B, Chen H, Guo N (2002) Flow–injection chemiluminescence determination of ascorbic acid by use of the cerium(IV)–Rhodamine B system. Anal Chim Acta 464(2):289–293
8. He P, Niu Y, Mei Z-h, Bao J-f, Sun X-m (2010) Measurement of ascorbic acid in single rat peritoneal mast cells using capillary electrophoresis with electrochemical detection. J Chromatogr B 878(15):1093–1097
9. Cheng H, Wang X, Wei H (2015) Ratiometric electrochemical sensor for effective and reliable detection of ascorbic acid in living brains. Anal Chem 87(17):8889–8895
10. Arabi M, Ostovan A, Wang Y, Mei R, Fu L, Li J, Wang X, Chen L (2022) Chiral molecular imprinting-based SERS detection strategy for absolute enantiomeric discrimination. Nat Commun 13(1):5757
11. Arabi M, Chen L (2022) Technical challenges of molecular-imprinting-based optical sensors for environmental pollutants. Langmuir 38(19):5963–5967
12. Arabi M, Ostovan A, Zhang Z, Wang Y, Mei R, Fu L, Wang X, Ma J, Chen L (2021) Label-free SERS detection of Raman-Inactive protein biomarkers by Raman reporter indicator: Toward ultrasensitivity and universality. Biosens Bioelectron 174:112825
13. Li X, Zhu H, Liu P, Wang M, Pan J, Qiu F, Ni L, Niu X (2021) Realizing selective detection with nanozymes: Strategies and trends. Trac-trend Anal Chem 143:116379
14. Liang M, Yan X (2019) Nanozymes: from new concepts, mechanisms, and standards to applications. Accounts Chem Res 52(8):2190–2200
15. Chong Y, Liu Q, Ge C (2021) Advances in oxidase-mimicking nanozymes: classification, activity regulation and biomedical applications. Nano Today 37:101076
16. Attar F, Shahpar MG, Rasti B, Sharifi M, Saboury AA, Rezayat SM, Falahati M (2019) Nanozymes with intrinsic peroxidase-like activities. J Mol Liq 278:130–144
17. Chen Z-J, Huang Z, Sun Y-M, Xu Z-L, Liu J (2021) The most active oxidase-mimicking mn_2o_3 nanozyme for biosensor signal generation. Chem A Europ J 27(37):9597–9604
18. Fu R, Zhou J, Wang Y, Liu Y, Liu H, Yang Q, Zhao Q, Jiao B, He Y (2021) Oxidase-like nanozyme-mediated altering of the aspect ratio of gold nanorods for breaking through H_2O_2-supported multicolor colorimetric assay: application in the detection of acetylcholinesterase activity and its inhibitors. ACS Appl Bio Mater 4(4):3539–3546
19. Liu J, Meng L, Fei Z, Dyson PJ, Zhang L (2018) On the origin of the synergy between the Pt nanoparticles and MnO_2 nanosheets in Wonton-like 3D nanozyme oxidase mimics. Biosens Bioelectron 121:159–165
20. Liu B, Huang Z, Liu J (2016) Boosting the oxidase mimicking activity of nanoceria by fluoride capping: rivaling protein enzymes and ultrasensitive F^- detection. Nanoscale 8(28):13562–13567
21. Li D, Liu B, Huang P-JJ, Zhang Z, Liu J (2018) Highly active fluorogenic oxidase-mimicking NiO nanozymes. Chem Commun 54(88):12519–12522
22. Wang L, Ye K, Pan J, Song H, Li X, Niu X (2019) A catalytic reaction-based colorimetric assay of alkaline phosphatase activity based on oxidase-like MnO_2 microspheres. Anall Methods 11(42):5472–5477
23. Wang J, Tao H, Lu T, Wu Y (2021) Adsorption enhanced the oxidase-mimicking catalytic activity of octahedral-shape Mn_3O_4 nanoparticles as a novel colorimetric chemosensor for ultrasensitive and selective detection of arsenic. J Colloid Interf Sci 584:114–124
24. Ganganboina AB, Doong R-a (2018) The biomimic oxidase activity of layered V2O5 nanozyme for rapid and sensitive nanomolar detection of glutathione. Sensor Actuat B-Chem 273:1179–1186
25. Zhang T, Xing Y, Song Y, Gu Y, Yan X, Lu N, Liu H, Xu Z, Xu H, Zhang Z, Yang M (2019) AuPt/MOF-graphene: a synergistic catalyst with surprisingly high peroxidase-like activity and its application for H_2O_2 Detection. Anal Chem 91(16):10589–10595
26. Chen C, Xie M, Kong L, Lu W, Feng Z, Zhan J (2020) Mn3O4 nanodots loaded g-C3N4 nanosheets for catalytic membrane degradation of organic contaminants. J Hazard Mater 390:122146
27. Li Z, Yang X, Yang Y, Tan Y, He Y, Liu M, Liu X, Yuan Q (2018) Peroxidase-mimicking nanozyme with enhanced activity and high stability based on metal-support interactions. Chem-Eur J 24(2):409–415
28. Ahmed SR, Takemeura K, Li T-C, Kitamoto N, Tanaka T, Suzuki T, Park EY (2017) Size-controlled preparation of peroxidase-like graphene-gold nanoparticle hybrids for the visible detection of norovirus-like particles. Biosens Bioelectron 87:558–565
29. Chen X, Zhai N, Snyder JH, Chen Q, Liu P, Jin L, Zheng Q, Lin F, Hu J, Zhou H (2015) Colorimetric detection of Hg^{2+} and Pb^{2+} based on peroxidase-like activity of graphene oxide–gold nanohybrids. Anall Methods 7(5):1951–1957
30. Darabdhara G, Boruah PK, Das MR (2018) Colorimetric determination of glucose in solution and via the use of a paper strip by exploiting the peroxidase and oxidase mimicking activity of bimetallic Cu-Pd nanoparticles deposited on reduced graphene oxide, graphitic carbon nitride, or MoS_2 nanosheets. Microchim Acta 186(1):13
31. Borthakur P, Boruah PK, Das MR (2021) CuS and NiS nanoparticle-decorated porous-reduced graphene oxide sheets as efficient peroxidase nanozymes for easy colorimetric detection of Hg(II) ions in a water medium and using a paper strip. ACS Sustain Chem Eng 9(39):13245–13255
32. Wang Q, Zhang X, Huang L, Zhang Z, Dong S (2017) One-pot synthesis of Fe_3O_4 nanoparticle loaded 3D porous graphene nanocomposites with enhanced nanozyme activity for glucose detection. ACS Appl Mater Interfaces 9(8):7465–7471
33. Borthakur P, Darabdhara G, Das MR, Boukherroub R, Szunerits S (2017) Solvothermal synthesis of CoS/reduced porous graphene oxide nanocomposite for selective colorimetric detection of Hg(II) ion in aqueous medium. Sensor Actuat B-Chem 244:684–692
34. Chu Z, Xiao M, Dong Q, Li G, Hu T, Zhang Y, Jiang Z (2023) Porous reduced graphene oxide for ultrasensitive detection of nitrogen dioxide. Chin Chem Lett 34(1):107197
35. Zhang N, Ning X, Chen J, Xue J, Lu G, Qiu H (2022) Photocatalytic degradation of tetracycline based on the highly reactive interface between graphene nanopore and TiO_2 nanoparticles. Micropor Mesopor Mat 338:111958

36. Chen Z, Li Z, Chen J, Tan H, Wu J, Qiu H (2022) Selective adsorption of rare earth elements by Zn-BDC MOF/graphene oxide nanocomposites synthesized via in situ interlayer-confined strategy. Ind Eng Chem Res 61(4):1841–1849
37. Wu J, Li Z, Tan H, Du S, Liu T, Yuan Y, Liu X, Qiu H (2021) Highly selective separation of rare earth elements by Zn-BTC metal–organic framework/nanoporous graphene via in situ green synthesis. Anal Chem 93(3):1732–1739
38. Song L, Zhang H, Cai T, Chen J, Li Z, Guan M, Qiu H (2019) Porous graphene decorated silica as a new stationary phase for separation of sulfanilamide compounds in hydrophilic interaction chromatography. Chin Chem Lett 30(4):863–866
39. Chen J, Wang L, Huang Y, Li Z, Zhang H, Chand Ali M, Liu J, Chen X, Qiu H (2019) Fabrication of nanoporous graphene/cuprous oxide nanocomposite and its application for chemiluminescence sensing of NADH in human serum and cells. Sensor Actuat B-Chem 290:15–22
40. Hummers WS Jr, Offeman RE (1958) Preparation of graphitic oxide. J Am Chem Soc 80(6):1339–1339
41. Jiangying Q, Feng G, Quan Z, Zhiyu W, Han H, Beibei L, Wubo W, Xuzhen W, Jieshan Q (2013) Highly atom-economic synthesis of graphene/Mn_3O_4 hybrid composites for electrochemical supercapacitors. Nanoscale 5(7):2999–3005
42. Li Y, Qu J, Gao F, Lv S, Shi L, He C, Sun J (2015) In situ fabrication of Mn_3O_4 decorated graphene oxide as a synergistic catalyst for degradation of methylene blue. Appl Catal B-Environ 162:268–274
43. Bharath G, Arora N, Hai A, Banat F, Savariraj D, Taher H, Mangalaraja RV (2020) Synthesis of hierarchical Mn_3O_4 nanowires on reduced graphene oxide nanoarchitecture as effective pseudocapacitive electrodes for capacitive desalination application. Electrochim Acta 337:135668
44. Cheng C, Huang Y, Wang N, Jiang T, Hu S, Zheng B, Yuan H, Xiao D (2015) Facile fabrication of Mn_2O_3 nanoparticle-assembled hierarchical hollow spheres and their sensing for hydrogen peroxide. ACS Appl Mater Interfaces 7(18):9526–9533
45. Nana L, Ruiyi L, Qinsheng W, Yongqiang Y, Xiulan S, Guangli W, Zaijun L (2021) Colorimetric detection of chlorpyrifos in peach based on cobalt-graphene nanohybrid with excellent oxidase-like activity and reusability. J Hazard Mater 415:125752
46. Wang T, Le Q, Guo X, Huang M, Liu X, Dong F, Zhang J, Zhang YX (2019) Preparation of porous graphene@Mn_3O_4 and its application in the oxygen reduction reaction and supercapacitor. ACS Sustain Chem Eng 7(1):831–837